J Shoulder Elbow Surg (2021) 30, e199–e211

ELSEVIER

Journal of Shoulder and Elbow Surgery

www.elsevier.com/locate/ymse

Degenerative changes in the elbow joint after radial head excision for fracture: quantitative 3-dimensional analysis of bone density, stress distribution, and bone morphology

Satoshi Miyamura, MD, PhD[a,b,*], Jonathan Lans, MD[a], Tsuyoshi Murase, MD, PhD[b], Kunihiro Oka, MD, PhD[b], Neal C. Chen, MD[a]

[a]*Department of Orthopaedic Surgery, Hand and Upper Extremity Service, Massachusetts General Hospital, Harvard Medical School, Boston, MA, USA*
[b]*Department of Orthopaedic Surgery, Graduate School of Medicine, Osaka University, Suita, Osaka, Japan*

Hypothesis and background: Some investigators speculate that excision may lead to elbow arthritis and associated problems; however, evidence supporting this theory is limited. It is hypothesized that radial head excision causes bone density changes as a result of asymmetrical stress distributions, consequently leading to osteophyte formation. In this study, we sought to quantitatively compare the 3-dimensional (3D) bone density and stress distributions between operative and nonoperative elbows in patients who underwent radial head excision. Furthermore, we aimed to quantify the bone morphologic changes using 3D models in the same cohort.

Methods: After retrospective identification, this study enrolled 6 patients who had undergone radial head excision for radial head fractures. We created 3D bone models using computed tomography data obtained from the injured and uninjured elbows. Humerus and ulna models were divided into anatomic regions, and the bone density of each region was assessed and described by its percentage of high-density volume (%HDV). We also constructed finite element models and measured the stress values in each region. Furthermore, we compared the bone morphology by superimposing the operative elbow onto the mirror image of the nonoperative elbow.

Results: The mean interval from radial head excision to examination was 8.4 ± 3.3 years. The %HDV on the operative side was higher than that of the nonoperative side at the anterolateral trochlea (77.5% ± 6.5% vs. 64.6% ± 4.0%, $P = .028$) and posterolateral trochlea (70.7% ± 7.8% vs. 63.1% ± 3.8%, $P = .034$) regions of the distal humerus. Reciprocal changes were observed in the proximal ulna, as %HDV was higher in the lateral coronoid (52.6% ± 9.6% vs. 34.2% ± 6.6%, $P = .007$). The stress distributions paralleled the bone density measurements. The operative elbows demonstrated an enlarged capitellum and a widened and deepened trochlea with osteophyte formation compared with the nonoperative side.

Discussion and conclusion: In elbows treated with radial head excision, we identified asymmetrical bone density and stress alterations on the lateral side of the ulnohumeral joint and bone morphologic changes across the joint. These data support the theory that radial head excision contributes to ulnohumeral arthritis over the long term.

Level of evidence: Level III; Case-Control Design; Prognosis Study

Keywords: Bone density; osteoarthritis; osteophyte; radial head fracture; radial head excision; stress distribution; ulnohumeral joint

Institutional review board approval was received from Partners Human Research Committee (study no. 2019P000391).

*Reprint requests: Satoshi Miyamura, MD, PhD, Department of Orthopaedic Surgery, Hand and Upper Extremity Service, Massachusetts General Hospital, Harvard Medical School, Yawkey Center, 55 Fruit St, Ste 2100, Boston, MA 02114, USA; Department of Orthopaedic Surgery, Graduate School of Medicine, Osaka University, 2-2 Yamada-oka, Suita, Osaka 565-0871, Japan.

E-mail address: m1ttyd2s@ort.med.osaka-u.ac.jp (S. Miyamura).

1058-2746/$ - see front matter
https://doi.org/10.1016/j.jse.2020.09.035

Radial head excision is a surgical option for comminuted radial head fractures. Nonetheless, arthritic changes of the elbow following radial head excision are frequently reported,[9,17,35,42] with few analyses evaluating biomechanical changes. Additionally, it remains challenging to determine how the initiating trauma and radial head excision each contribute to the development of arthritis. Antuña et al[2] reported osteoarthritic changes in all 26 patients in their study with an isolated radial head fracture that underwent radial head excision, with little functional impairment at long-term follow-up. Subsequently, there has been debate in the setting of an isolated, irreparable comminuted head fracture on whether the cost of radial head arthroplasty is justified compared with excision.

Approximately 60% of the axial load of the forearm passes through the radial head,[18,34] and the radial head is an important valgus stabilizer of the elbow joint.[22,33,39] The absence of radiocapitellar contact theoretically alters loading by increasing the load through the ulnohumeral joint and reducing valgus stability, which can both contribute to degenerative changes. This might explain why arthritis develops after radial head excision, posing the argument for radial head preservation. Observational studies have suggested that preservation of the radial head may limit arthrosis compared with excision.[28] Prior studies have suggested that fixation of the radial head yields better functional outcomes but diminished elbow and forearm motions compared with radial head excision.[24]

Generally, degenerative change is characterized by altered subchondral bone density and is associated with mechanical stress across a joint.[6,10,16,40,41] Additionally, reactive osteophyte formation is commonly observed in osteoarthritic joints.[8,31] It is hypothesized that radial head excision causes bone density changes as a result of asymmetrical stress distributions, consequently leading to osteophyte formation. In this study, the aim was to quantitatively compare the 3-dimensional (3D) bone density and stress distributions between operative and nonoperative elbows in patients who underwent radial head excision. A secondary aim was to quantify the bone morphologic changes using 3D models in the same cohort.

Methods

Study setting

This case-control study evaluated 6 patients who underwent radial head excision for a radial head fracture. Patients were identified retrospectively for enrollment, and this study was performed at a single institutional hospital system in the Northeastern United States, including 5 urban hospitals, of which 2 were level 1 trauma centers. Patients' medical charts were reviewed to determine which patients to invite to return for clinical and radiographic evaluations. Written informed consent was obtained from all study participants.

Patient enrollment

Patients who underwent radial head excision were identified retrospectively using Current Procedural Terminology codes for radial head excision. A medical chart review of all relevant orthopedic encounters from January 2002 to December 2017 was performed, identifying 151 patients. Patients were included if they were aged $\geq$ 18 years and had undergone radial head excision for a radial head fracture after either acute or distant trauma $\geq$ 5 years prior to the date of enrollment. Patients were excluded if they had an elbow fracture-dislocation, a terrible-triad injury of the elbow, an Essex-Lopresti injury, rheumatoid arthritis, or a bilateral injury or were pregnant.

Medical records were screened by 2 experienced orthopedic elbow surgeons (>10 years of practice), identifying 28 adult patients who met the inclusion criteria. After 10 patients without accessible preoperative and postoperative radiographs were excluded, 18 eligible patients were contacted to participate in this study. We were able to contact 8 patients, who were screened by a telephone interview to determine whether they had additional treatment or trauma to the affected elbow. Six patients agreed to participate in this study and were enrolled (Fig. 1).

Patient clinical data collection

Study data were collected and managed using REDCap (Research Electronic Data Capture) tools hosted at our institution.[19] Demographic information included age, sex, race, height, weight, body mass index, dominant limb, and profession. Injury characteristics were also collected, including the mechanism of the initial injury, the Mason fracture classification,[29] and the interval from surgery to examination. Mason type was classified by 2 experienced orthopedic elbow surgeons. Elbow pain was graded as none, mild, moderate, or severe, and elbow stability was graded as stable, moderately unstable, or grossly unstable. Additional information was collected regarding the presence of ulnar nerve symptoms or wrist pain. Elbow (flexion and extension), forearm (supination and pronation), and wrist (flexion and extension) ranges of motion on both the operative and nonoperative sides were measured using a goniometer. The Quick Disabilities of the Arm, Shoulder and Hand (QuickDASH) score was used to assess patient-reported outcomes; the Mayo Elbow Performance Score (MEPS) was also calculated. Patients rated their satisfaction with treatment as very satisfied, satisfied, neither satisfied nor dissatisfied, dissatisfied, or very dissatisfied. All of the physical examinations were performed by a single experienced elbow surgeon.

Three-dimensional computed tomography model reconstruction

By use of a helical computed tomography (CT) scanner (Revolution CT; GE Healthcare, WI, USA), both elbows were scanned with full extension of the elbows and the forearms maintained in supination. We used a low–radiation dose technique (slice

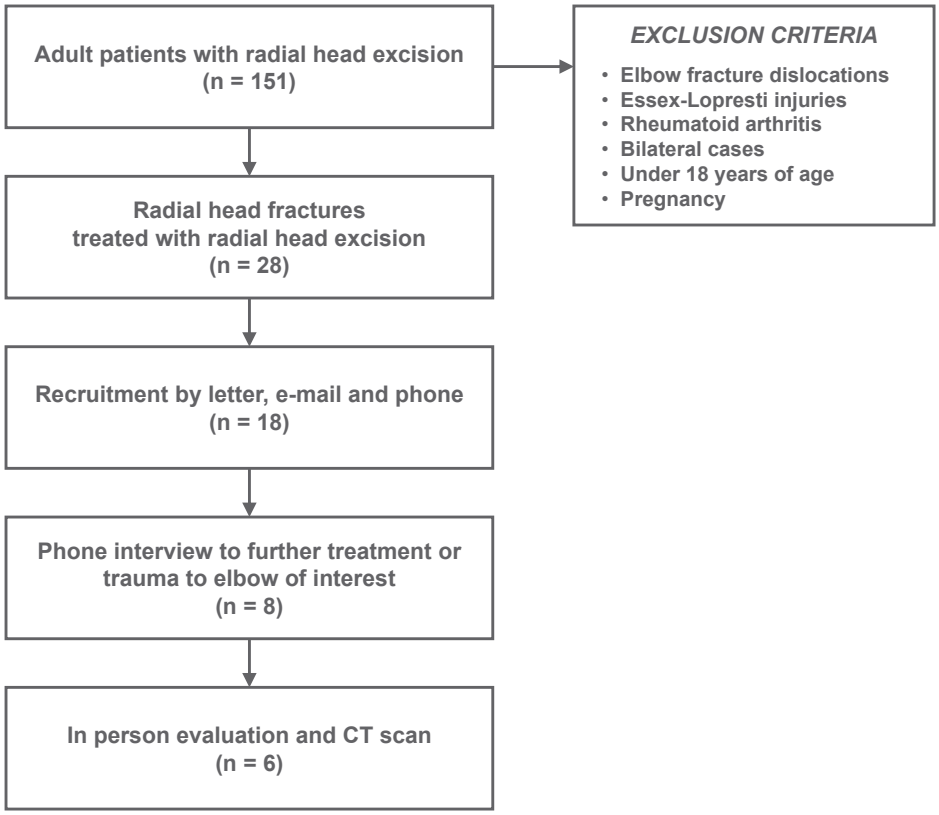

Figure 1 Flowchart of patient enrollment. *CT*, computed tomography.

thickness, 0.625 mm; pixel size, 0.40 mm; scan time, 0.5 seconds; scan pitch, 0.562:1; tube current, 20-150 mA; and tube voltage, 120 kV)[37]; with a total dosage of 0.2 mSv per scan. Digital data were saved and analyzed. The 3D surface models of the bilateral humerus, ulna, and radius were created by a semiautomatic segmenting technique using MvIndex/Bone Simulator image processing software (Orthree, Osaka, Japan).

Bone density measurement

As previously described, the orthogonal coordinate systems of the distal humerus (X-, Y-, and Z-axes) and proximal ulna (x-, y-, and z-axes) were determined.[26,32] The articular surface of the distal humerus was divided into 5 regions of interest (ROIs), and the articular surface of the proximal ulna was divided into 4 ROIs. The distal humerus was categorized into 5 regions: (1) capitellum, (2) anterolateral trochlea, (3) anteromedial trochlea, (4) posterolateral trochlea, and (5) posteromedial trochlea. The proximal ulna was categorized into 4 regions: (1) lateral coronoid, (2) medial coronoid, (3) lateral olecranon, and (4) medial olecranon[20,32] (Fig. 2, Supplementary Appendix S1).

The bone density of each ROI was analyzed using Mechanical Finder software (version 10.0; Research Center for Computational Mechanics, Tokyo, Japan). After the 3D bone models were meshed with 1.0-mm tetrahedral elements, the pixel intensity of each element was computed and the values of all elements in each ROI were averaged to give a result equivalent to the bone density.[32]

We calculated the percentage of high-density volume (% HDV), which was the percentage of the overall volume of the distal humerus or proximal ulna that had a bone density greater than the average density of all the ROIs of the respective bone.[32] The absolute values of bone density vary between patients. Because of this, we sought to describe relative bone density as a proportion of the high density in each ROI. These internal references helped resolve potential variation arising from scanning conditions and individual anatomy.[12]

Finite element analysis

We constructed subject-specific finite element models using Mechanical Finder software via meshed bone models that retained the pixel intensity. Regions of articular cartilage were defined as areas in the humerus, radius, and ulna models expanded by 2 mm.[30,32] Cartilage regions were also meshed with 1.0-mm tetrahedral elements.

On the basis of the material properties and the boundary conditions according to previous studies[5,15,21,23,27,30,32,44] (Fig. 3; detailed in Supplementary Appendix S2), the equivalent stress was measured and the values of all the elements at each ROI were averaged. For these data, we calculated the percentage of high-stress volume (%HSV), which was the percentage of the overall stress that demonstrated above-average stress across the respective bone.

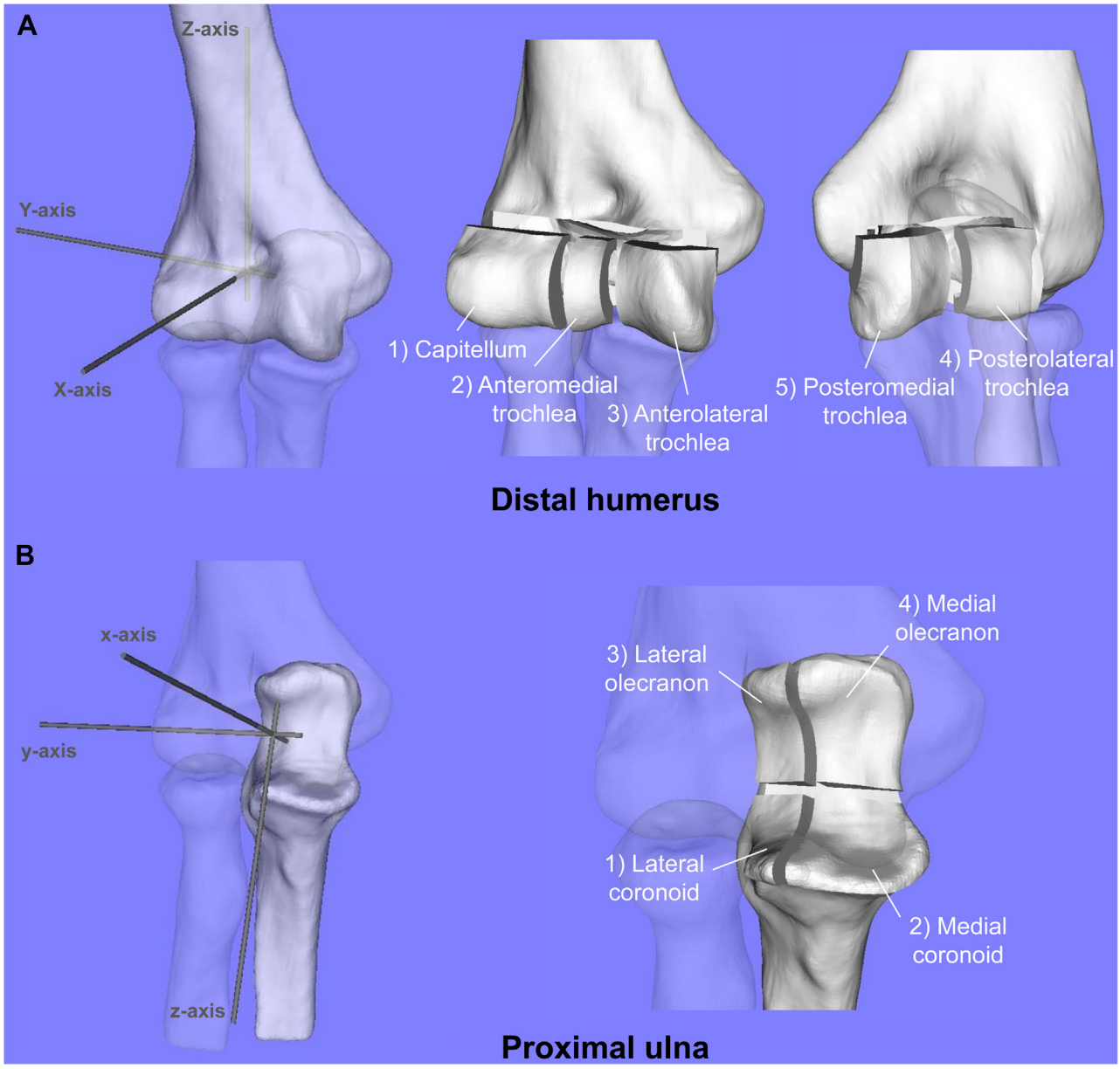

Figure 2 Orthogonal coordinate systems and regions of interest for distal humerus (**A**) and proximal ulna (**B**) (detailed in Supplementary Appendix S1).

Evaluation of bone morphology

The bone models of the operative side and mirror images of the nonoperative side were superimposed with a surface-based registration technique using an iterative closest point algorithm.[3,4,25] Bone morphology was evaluated by measuring a minimum interval distance between the models in the cross-sectional planes around the Y- or y-axis. In the distal humerus, measurements were performed at the greatest convexity of the capitellum, lateral trochlea, and medial trochlea and categorized into the anterior and posterior portions (Figs. 4, *A* and *B*). In the proximal ulna, measurements were performed at the lateral and medial verges of the ulnar trochlea, along with the coronoid and olecranon tips, and categorized into the anterior and posterior portions (Fig. 4, *C*).

Three-dimensional analysis of proximal radius migration

We quantified 3D migration by calculating the spatial movement of the radius relative to the ulna using a surface-based registration technique.[3,25] The amount of spatial translation was calculated and divided into proximal, medial, and posterior directions based on the orthogonal coordinate system of the proximal ulna (Fig. 5).

Statistical analysis

SPSS software (version 24.0; IBM, Armonk, NY, USA) was used to perform the statistical analyses. Significance was set at $P < .05$

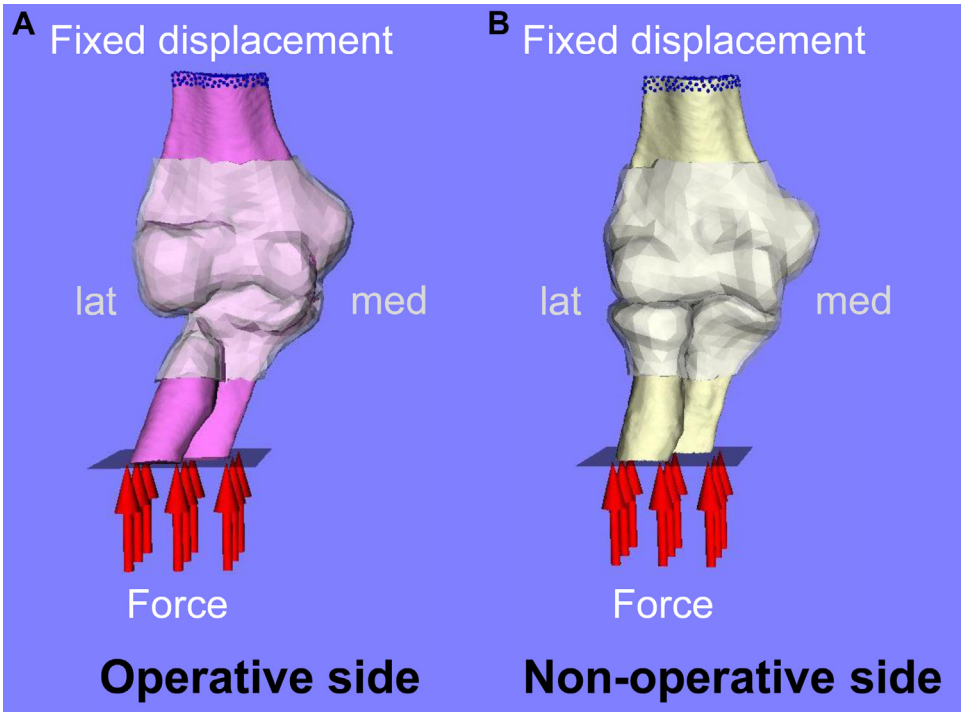

Figure 3 Diagrams of boundary conditions: 3-dimensional elbow models of operative side (*purple*; **A**) and nonoperative side (*beige*; **B**). *lat*, lateral; *med*, medial.

for all tests. The normality of each variable was assessed with the Shapiro-Wilk test. In each ROI, values of the %HDV and %HSV were compared between the operative and nonoperative sides using the paired *t* test or Wilcoxon signed rank test.

Regarding osteophyte formation, measurements of the anterior and posterior parts of the humerus were compared among the capitellum, lateral trochlea, and medial trochlea using 1-way analysis of variance with the post hoc Tukey test. Measurements of the coronoid and olecranon were compared between the lateral trochlea and medial trochlea using the unpaired *t* test.

Because there are no similar data of which are aware, we conducted a post hoc power analysis for the Wilcoxon signed rank test ($\alpha = .05$, 2-tailed) using the effect size calculated from the bone density measurements at the anterolateral trochlea in the operative and nonoperative elbows ($n = 6$ for each) to test the primary hypothesis. On the basis of this, the power ($1 - \beta$) achieved to identify meaningful differences was ≥ 0.99. This calculation was performed using the G*Power program (Universität Kiel, Kiel, Germany).

Results

Patient characteristics

The patient characteristics are presented in Table I. The mean age at the examination was 55.2 ± 17.1 years, and the mean interval from radial head excision to CT was 8.4 ± 3.3 years. Three patients underwent primary radial head excision for fractures. Two patients underwent secondary radial head excision for restricted forearm rotation and crepitation, at 4 and 5 years after an initial osteosynthesis. One patient underwent radial head excision without prior surgery owing to collapse of the radial head 10 years after the initial injury. In the 3 patients who underwent excision after distant trauma, a symmetrical, preserved ulnohumeral joint space was seen at the time of excision. The average QuickDASH score and MEPS were 21.6 ± 22.3 points and 88.3 ± 13.3 points, respectively. All 6 patients had limitations of elbow extension; the mean flexion contracture was 22° ± 5° compared with the nonoperative side. No patient had instability at the time of excision.

The mean 3D migration of the radius on the operative side was 3.0 ± 3.8 mm in the proximal direction, 2.6 ± 4.3 mm in the medial direction, and 1.8 ± 3.1 mm in the posterior direction.

Bone density analysis

In the distal humerus, the %HDV on the operative side was higher than that on the nonoperative side at the anterolateral trochlea (77.5% ± 6.5% vs. 64.6% ± 4.0%, $P = .028$), posterolateral trochlea (70.7% ± 7.8% vs. 63.1% ± 3.8%, $P = .034$), and posteromedial trochlea (64.1% ± 2.6% vs. 56.9% ± 4.5%, $P = .002$). Conversely, the %HDV on the operative side was lower than that on the nonoperative side in the capitellum (20.8% ± 10.1% vs. 38.2% ± 9.4%, $P = .025$) (Fig. 6, *A* and *B*; Table II).

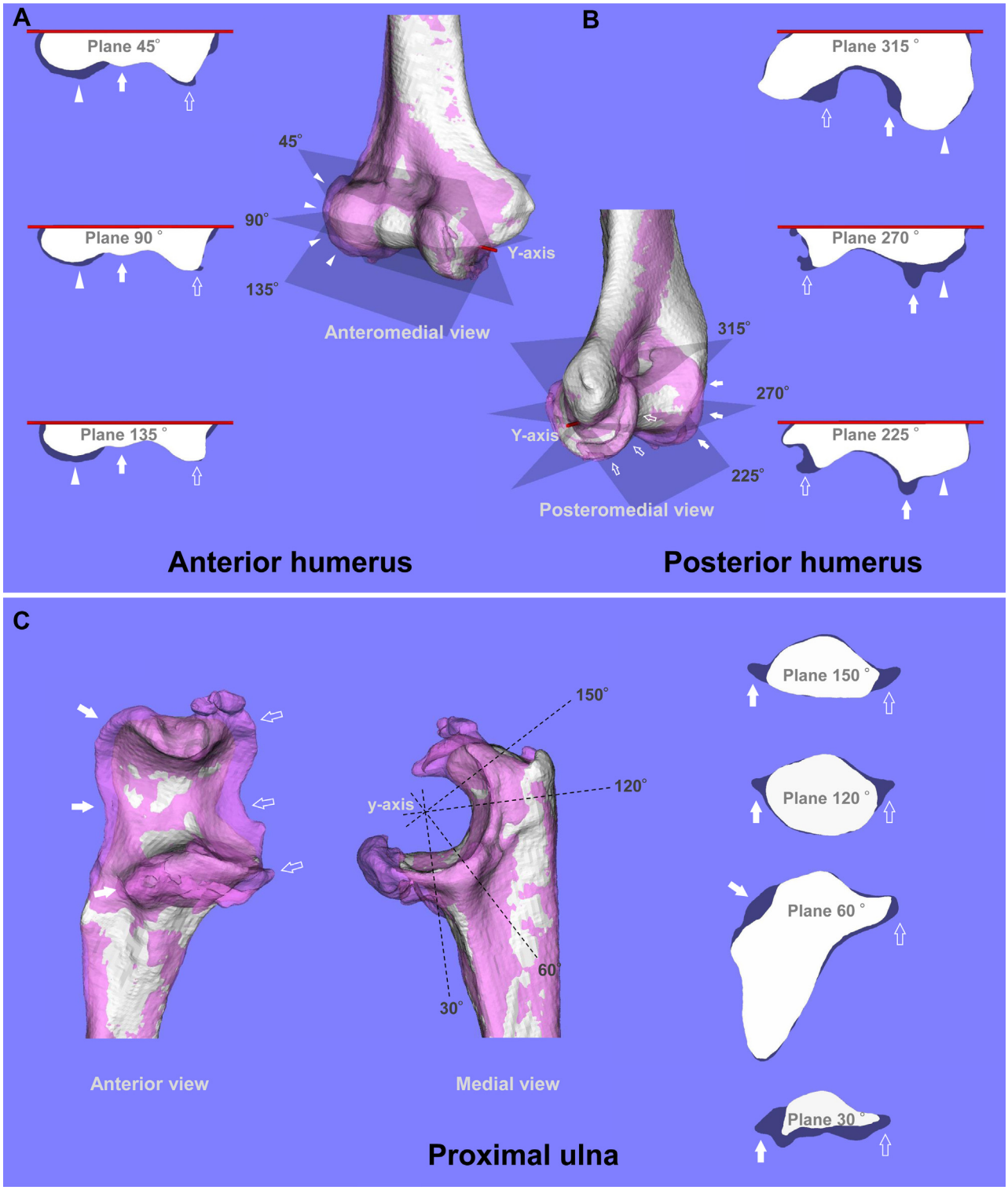

Figure 4 Superimposed 3-dimensional models of the operative side (*purple*) and mirror images of the nonoperative side (*white*) and their cross-sectional planes showing the greatest convexity of the capitellum (*arrowheads*), lateral trochlea verge (*filled arrows*), and medial trochlea verge (*open arrows*). In the distal humerus, the Y-Z plane is incrementally increased by 45° around the Y-axis, and 3 planes of interest are determined: 45° (225°) plane, 90° (270°) plane, and 135° (315°) plane. In the proximal ulna, the y-z plane is incrementally increased by 30° around the y-axis, and 4 planes of interest are determined: 30° (210°) plane, 60° (240°) plane, 120° (300°) plane, and 150° (330°) plane. (**A**) Anterior part of distal humerus (45°, 90°, and 135° planes). (**B**) Posterior part of distal humerus (225°, 270°, and 315° planes). (**C**) Anterior portion (30° and 60° planes) and posterior portion (120° and 150° planes) of proximal ulna.

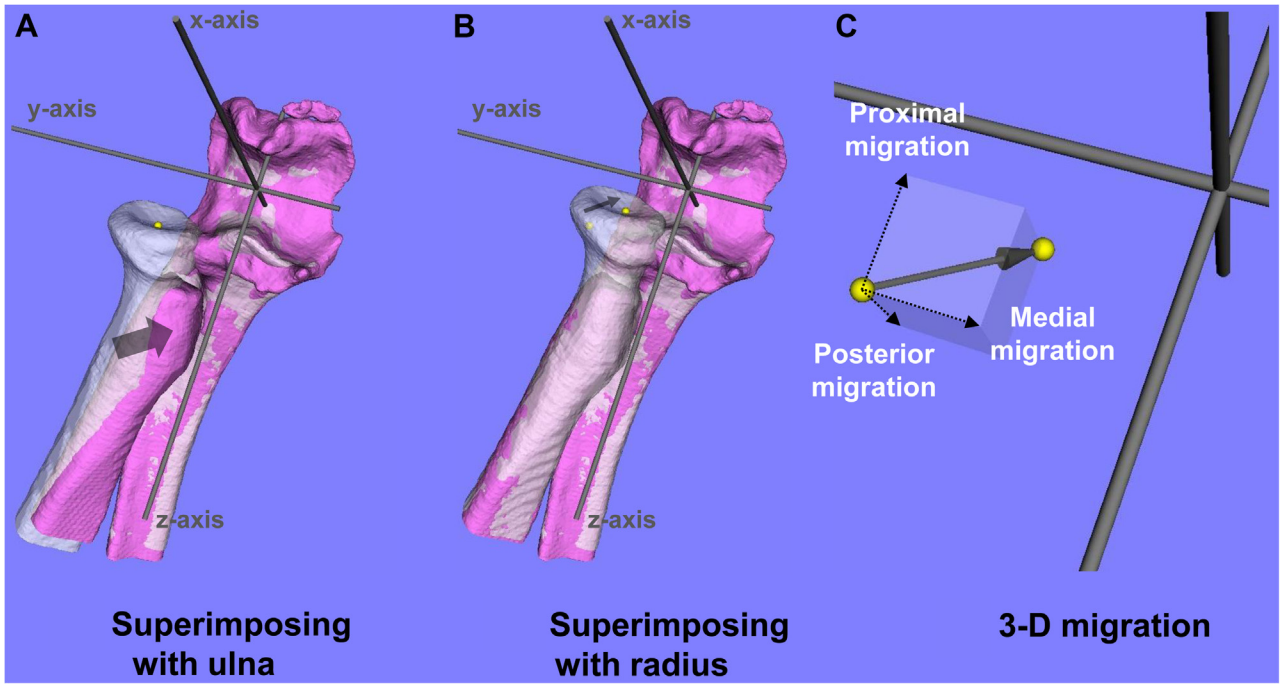

Figure 5 Schemas of 3-dimensional *(3-D)* analysis of proximal radius migration. (**A**) The forearm bones on the operative side and the mirror image of the nonoperative side are superimposed with the ulna. (**B**) The radius of the mirror image of the nonoperative side is superimposed onto the bones on the operative side with the radius, and the movement of the center of the radial head is tracked. (**C**) Consequently, the amount of translation is calculated and divided into proximal, medial, and posterior directions based on the orthogonal coordinate system of the proximal ulna.

In the proximal ulna, the %HDV on the operative side was higher than that on the nonoperative side in the lateral coronoid (52.6% ± 9.6% vs. 34.2% ± 6.6%, $P = .007$) whereas the %HDV on the operative side was lower than that on the nonoperative side in the lateral olecranon (41.6% ± 6.7% vs. 55.4% ± 8.3%, $P = .011$) (Fig. 6, *C*; Table II).

Finite element analysis

The finite element analysis results paralleled the bone density measurements (Fig. 7, Table III). In the distal humerus, the %HSV on the operative side was higher than that on the nonoperative side in the anterolateral trochlea (81.8% ± 7.7% vs. 64.0% ± 8.5%, $P = .022$) and posterolateral trochlea (74.1% ± 10.3% vs. 55.4% ± 12.6%, $P = .037$). Conversely, the %HSV on the operative side was lower than that on the nonoperative side in the capitellum (17.4% ± 10.2% vs. 47.5% ± 11.4%, $P = .007$). In the proximal ulna, the %HSV on the operative side was higher than that on the nonoperative side in the lateral coronoid (57.7% ± 10.1% vs. 43.0% ± 9.4%, $P = .041$).

Bone morphologic analysis

The largest anterior distal humerus osteophytes were observed around the capitellum (2.1 ± 0.7 mm); these were larger than those around the lateral trochlea (0.6 ± 0.4 mm, $P = .002$) or medial trochlea (1.2 ± 0.8 mm, $P = .048$). The largest posterior distal humerus osteophytes were observed at the lateral trochlea (2.9 ± 1.2 mm, $P = .008$) and medial trochlea (3.5 ± 1.4 mm); both of these were larger than those around the capitellum (0.6 ± 0.5 mm, $P = .001$) (Table IV).

In the coronoid, the measurement of osteophyte formation around the lateral trochlea (4.0 ± 1.5 mm) was larger than that around the medial trochlea (2.2 ± 0.6 mm, $P = .032$). The average height of the coronoid tip was 5.0 ± 3.7 mm. In the olecranon, the measurement of osteophyte formation around the medial trochlea was 2.1 ± 1.2 mm and that around the lateral trochlea was 3.3 ± 1.9 mm. The average height of the olecranon tip was 4.5 ± 2.0 mm (Table V).

Discussion

Using bilateral elbow CT data, we quantitatively analyzed the bone density, stress distribution, and bone morphology in the elbow joints of 6 patients who underwent radial head excision for radial head fractures and compared this with the uninjured elbows in the same patients. The results showed an increased bone density and stress concentration on the lateral side of the ulnohumeral joint following radial

Table I Patient data

	Mason type	Age at CT, yr	Sex	Race	Height, cm	Weight, kg	BMI	Dominant limb	Operative side	Profession	Interval from excision to CT, yr	Elbow pain	Elbow instability
Case 1	2	48	M	White	180.3	106.6	32.8	R	R	Mechanic	12.5	Moderate	Stable
Case 2	3	41	F	White	175.2	128.4	41.8	R	L	Unemployed	6.8	None	Moderate instability
Case 3	3	32	M	Asian	181.6	68.0	20.6	R	L	Stagehand	5.2	None	Stable
Case 4	3	68	M	White	172.7	90.3	30.3	R	L	Unemployed	12.7	Mild	Moderate instability
Case 5	3	71	F	African American	160.0	78.0	30.5	R	R	Unemployed	6.8	None	Moderate instability
Case 6	2	71	F	White	165.1	84.8	31.1	R	L	Unemployed	6.5	None	Moderate instability
Mean		55.2			172.5	92.7	31.2				8.4		
SD		17.1			8.5	21.7	6.8				3.3		

head excision. We also found an enlarged capitellum and a widened and deepened trochlea with osteophyte formation in the elbow that underwent radial head excision compared with the nonoperative side.

Several studies have demonstrated satisfactory outcomes after radial head excision. Many of these have noted an increased incidence of radiographic arthritis at long-term follow-up.[2,9,17,24,35,38] Biomechanical and clinical studies have reinforced that the radial head and radiocapitellar contact contribute to elbow stability and function even though the radial head is conceptualized as a secondary stabilizer to valgus stress.[18,24,34,41]

In our study, elbows in which the radial head was excised had different bone density and stress distribution patterns compared with the nonoperative elbows. In the distal humerus on the operative side, the lateral and posteromedial trochlea had higher bone density and loading stress. Furthermore, the findings were suggestive of a bone density increase along the lateral aspect of the trochlea compared with the medial aspect when the differences among ROIs were analyzed. In the region directly opposing the lateral trochlea, the lateral coronoid and medial olecranon also had increased bone density and stress.

Prior studies have demonstrated that subchondral bone density reflects the stress acting on joint surfaces under actual loading conditions[14,36] and that subchondral bone changes reflect the development of osteoarthritis.[7,13,43] The bone density and stress changes identified in our study suggest that there is an increased valgus load through the ulnohumeral joint when the radial head is excised, subsequently leading to arthritis. In particular, the preferential bone density increase at the lateral aspect of the humeral trochlea suggests that the valgus stress tilts the ulna into the trochlea, resulting in uneven wear of the ulnohumeral cartilage (Fig. 8).

Regarding the morphologic bone analysis, our results demonstrated an enlarged capitellum and a widened and deepened trochlea. This bone reaction and osteophyte formation might occur in response to valgus instability and shear forces across the joint.[31] Furthermore, osteophytes may form at the lateral trochlea of the coronoid to reduce abnormal joint stress. It is notable that in prior studies evaluating elbow arthritis, the enlargement of the capitellum was rarely observed in elbows with primary arthritis, which typically demonstrate a wear pattern of this region.[1,11] It remains unclear why the capitellum enlarges, but we hypothesize that the trochlear overload from valgus stress stimulates enlargement of the lateral ridge, making the capitellum seem wider and flatter.

This study had some limitations. First, we were unable to perform direct comparison with radial head fractures treated with open reduction–internal fixation or prosthetic replacement because metal artifact would interfere with CT scanning. A similar comparison of patients undergoing open reduction–internal fixation or prosthetic replacement of the radial head is needed to gain further understanding but remains challenging given the radiographic artifact due to metallic arthroplasty. We hope future advances in CT metal suppression will make it possible to apply these techniques to patients who undergo radial head arthroplasty. Second, 3 patients had undergone radial head excision after distant trauma. However, we do not believe that the difference in the interval from injury to excision altered the findings substantially because they showed a symmetrical, preserved ulnohumeral joint space at the time of excision and the results of these 3 patients and those of the

Table I Patient data (*continued*)

Ulnar nerve symptom	Wrist pain	ROM (operative side/nonoperative side), °						Patient satisfaction	QuickDASH score, points	MEPS, points
		Elbow		Forearm		Wrist				
		Flexion	Extension	Supination	Pronation	Flexion	Extension			
Severe	None	110/135	−30/0	70/70	80/90	50/60	75/75	Dissatisfied	38.6	65
None	None	135/130	−22/−5	70/70	90/90	45/45	60/60	Satisfied	0	95
Moderate	None	125/130	−25/−5	60/80	70/70	60/75	60/65	Neither satisfied nor dissatisfied	9.1	100
Moderate	None	140/140	−25/0	85/75	80/80	60/60	70/65	Neither satisfied nor dissatisfied	27.3	80
None	None	125/150	−25/−5	80/70	70/80	75/60	60/60	Very satisfied	0	95
Moderate	None	120/130	−20/−10	70/80	70/70	65/65	50/60	Very satisfied	54.5	95
		126/136	−25/−3	73/74	77/80	59/61	63/64		21.6	88.3
		11/8	3/3	9/5	8/9	10/10	9/6		22.3	13.3

CT, computed tomography; *BMI*, body mass index; *ROM*, range of motion; *QuickDASH*, Quick Disabilities of the Arm, Shoulder and Hand; *MEPS*, Mayo Elbow Performance Score; *M*, male; *R*, right; *F*, female; *L*, left; *SD*, standard deviation.

other patients appeared similar. Third, our data do not allow one to make a definitive conclusion that radial head excision leads to arthritis. It is indeterminate whether these findings are directly related to the radial head excision or the chondrocyte injury at the time of the initial injury without having a comparison with the retained radial head, which is not feasible because of the CT methodology. Finally, the sample size was insufficient to compare clinical outcomes among patients to identify factors impacting outcomes. We did, however, have enough power to compare our modeling data; despite the cohort only consisting of 6 patients, our post hoc power analysis demonstrated a power of 0.99 based on data of bone density measurements at the anterolateral trochlea.

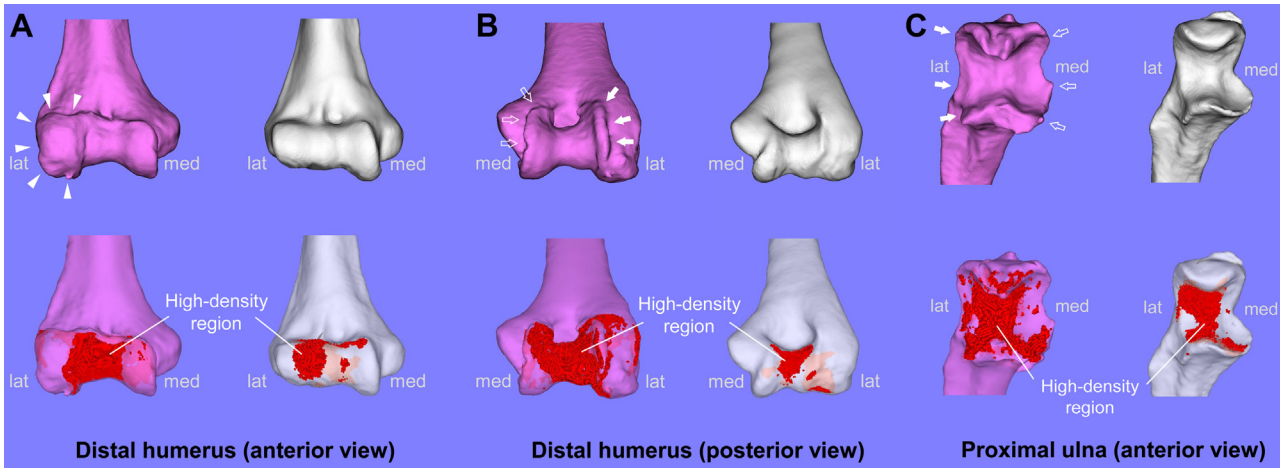

Figure 6 Three-dimensional bone models and distribution patterns of high–bone density region, showing operative side (*purple*) and mirror image of nonoperative side (*white*). (**A**) Anterior view of distal humerus. Enlargement of the capitellum (*arrowheads*) and distribution of the high-density region on the lateral side of the humeral trochlea are shown on the operative side when compared with the nonoperative side. (**B**) Posterior view of distal humerus. Osteophyte formation at the lateral trochlea verge (*filled arrows*) and medial trochlea verge (*open arrows*) and distribution of the high-density region on the entire surface of the humeral trochlea are shown on the operative side when compared with the nonoperative side. (**C**) Anterior view of proximal ulna. Osteophyte formation at the lateral trochlea verge (*filled arrows*) and medial trochlea verge (*open arrows*) and anterolateral distribution of the high-density region on the ulnar trochlea are shown on the operative side when compared with the nonoperative side. *lat*, lateral; *med*, medial.

Table II Percentage of HDV by region of distal humerus and proximal ulna

	Operative side, %	Nonoperative side, %	*P* value
Distal humerus			
Capitellum	20.8 ± 10.1	38.2 ± 9.4	.025*
Anterolateral trochlea	76.1 (74.4-76.9)	64.6 ± 4.0	.028†
Anteromedial trochlea	49.8 ± 12.8	51.8 ± 7.6	.753
Posterolateral trochlea	70.7 ± 7.8	63.1 ± 3.8	.034†
Posteromedial trochlea	64.1 ± 2.6	56.9 ± 4.5	.002†
Proximal ulna			
Lateral coronoid	52.6 ± 9.6	34.2 ± 6.6	.007†
Medial coronoid	49.0 ± 8.6	46.7 ± 5.8	.411
Lateral olecranon	41.6 ± 6.7	55.4 ± 8.3	.011*
Medial olecranon	46.3 ± 3.6	55.2 ± 11.5	.093

HDV, high-density volume.

Data with a normal distribution are presented as mean ± standard deviation, whereas those with a non-normal distribution are presented as median (interquartile range).

* The percentage of HDV was significantly lower for the operative side than the nonoperative side ($P < .05$).

† The percentage of HDV was significantly higher for the operative side than the nonoperative side ($P < .05$).

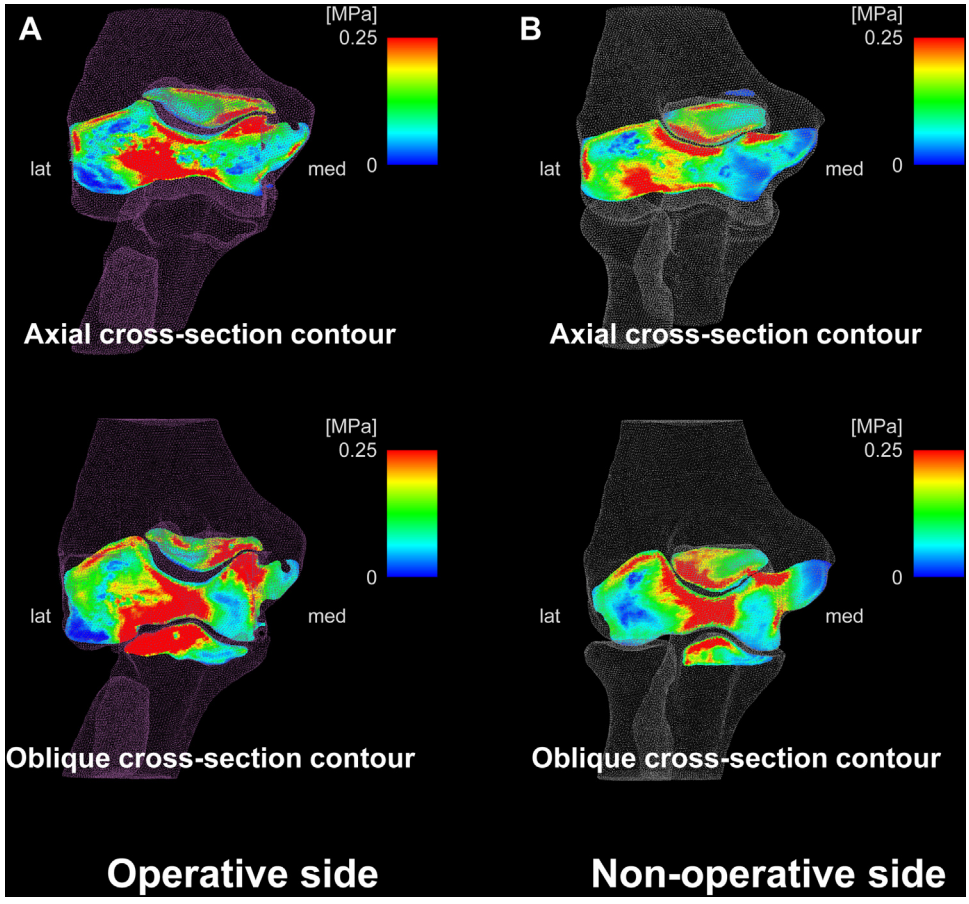

Figure 7 Contours of stress distributions: operative side (*purple mesh*; **A**) and mirror image of nonoperative side (*white mesh*; **B**). Stress contours are shown on cross sections of the axial plane (*top*) and anterior oblique plane to the humeral axis (*bottom*). In the operative elbow, loading caused stress to concentrate on the lateral side of the humeral trochlea and the lateral side of the coronoid when compared with the nonoperative elbow. *lat*, lateral; *med*, medial.

Table III Percentage of HSV by region of distal humerus and proximal ulna

	Operative side, %	Nonoperative side, %	*P* value
Distal humerus			
Capitellum	17.4 ± 10.2	47.5 ± 11.4	.007*
Anterolateral trochlea	81.8 ± 7.7	64.0 ± 8.5	.022†
Anteromedial trochlea	18.3 ± 12.3	9.9 ± 3.2	.128
Posterolateral trochlea	74.1 ± 10.3	55.4 ± 12.6	.037†
Posteromedial trochlea	42.5 ± 7.3	32.2 ± 14.0	.084
Proximal ulna			
Lateral coronoid	57.7 ± 10.1	43.0 ± 9.4	.041†
Medial coronoid	21.6 ± 10.6	11.2 ± 7.8	.101
Lateral olecranon	49.3 ± 11.5	52.0 ± 14.6	.538
Medial olecranon	45.2 ± 16.4	28.4 ± 4.1	.069

HSV, high-stress volume.
Data with a normal distribution are presented as mean ± standard deviation.
* The percentage of HSV was significantly lower for the operative side than the nonoperative side ($P < .05$).
† The percentage of HSV was significantly higher for the operative side than the nonoperative side ($P < .05$).

Table IV Bone morphologic analysis of distal humerus

Distal humerus	Region, mean ± SD, mm			*P* value		
	Capitellum	Lateral trochlea	Medial trochlea	Capitellum vs. lateral trochlea	Capitellum vs. medial trochlea	Lateral trochlea vs. medial trochlea
Anterior part	2.1 ± 0.7	0.6 ± 0.4	1.2 ± 0.8	.002*	.048*	.312
Posterior part	0.6 ± 0.5	2.9 ± 1.2	3.5 ± 1.4	.008†	.001†	.639

SD, standard deviation.
* The measurement was significantly higher for the capitellum than the trochlea ($P < .05$).
† The measurement was significantly higher for the trochlea than the capitellum ($P < .05$).

Table V Bone morphologic analysis of proximal ulna

Proximal ulna	Region, mean ± SD, mm		*P* value
	Lateral trochlea	Medial trochlea	
Coronoid	4.0 ± 1.5	2.2 ± 0.6	.032*
Olecranon	2.1 ± 1.2	3.3 ± 1.9	.226

SD, standard deviation.
* Significant difference ($P < .05$).

Conclusion

Radial head excision leads to altered bone density and morphology of the elbow joint probably as a result of changes in stress distributions through the ulnohumeral joint. These data support the theory that radial head excision contributes to ulnohumeral arthritis over the long term.

Acknowledgments

The authors thank clinical research coordinators Rachel Gottlieb, BSc, and Kiera Nysha Lunn, BSc, for their assistance with organization and subject tracking.

Disclaimer

This investigator-initiated study was supported by Acumed (USA, grant no. 233993) and Japan Elbow Society (Japan, grant no. JES201802); however, there are no conflicts of interest to declare.

Satoshi Miyamura received personal fees from Japan Elbow Society.

Jonathan Lans received personal fees from AxoGen.

Neal C. Chen received personal fees from Flexion Medical, Miami Device Solutions, DePuy Synthes, AO International, Skeletal Dynamics, OMeGA, and Acumed.

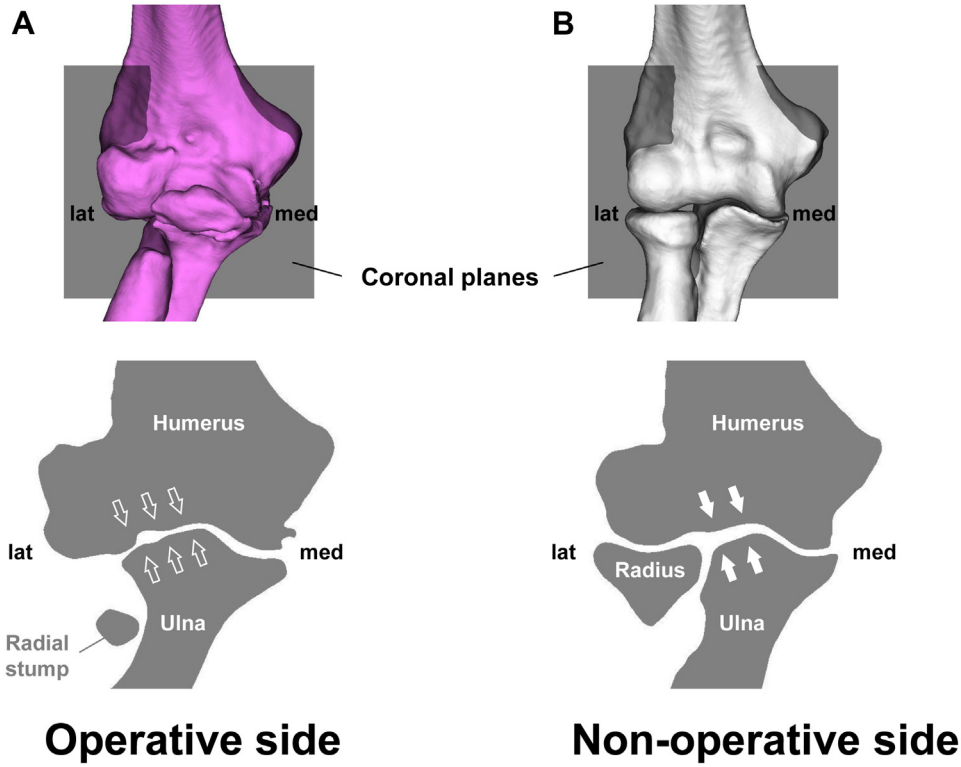

Figure 8 Three-dimensional bone models (*top*) and cross-sectional images (*bottom*) of operative side (*purple*; **A**) and mirror image of nonoperative side (*white*; **B**). The cross-sectional images are obtained by sectioning in the coronal plane. In the operative elbow, the ulnohumeral joint shows abnormal narrowing and widening at the lateral aspects (*open arrows*) when compared with the nonoperative side (*filled arrows*). *lat*, lateral; *med*, medial.

The other authors, their immediate families, and any research foundations with which they are affiliated have not received any financial payments or other benefits from any commercial entity related to the subject of this article.

Supplementary data

Supplementary data to this article can be found online at https://doi.org/10.1016/j.jse.2020.09.035.

References

1. Ahrens PM, Redfern DR, Forester AJ. Patterns of articular wear in the cadaveric elbow joint. J Shoulder Elbow Surg 2001;10:52-6.
2. Antuña SA, Sanchez-Marquez JM, Barco R. Long-term results of radial head resection following isolated radial head fractures in patients younger than forty years old. J Bone Joint Surg Am 2010;92:558-66. https://doi.org/10.2106/jbjs.i.00332
3. Audette MA, Ferrie FP, Peters TM. An algorithmic overview of surface registration techniques for medical imaging. Med Image Anal 2000;4:201-17.
4. Besl P, McKay N. A method for registration of 3D shapes. IEEE Trans Patt Anal 1992;14:239-56.
5. Bessho M, Ohnishi I, Matsuyama J, Matsumoto T, Imai K, Nakamura K. Prediction of strength and strain of the proximal femur by a CT-based finite element method. J Biomech 2007;40:1745-53. https://doi.org/10.1016/j.jbiomech.2006.08.003
6. Block JA, Shakoor N. Lower limb osteoarthritis: biomechanical alterations and implications for therapy. Curr Opin Rheumatol 2010;22:544-50. https://doi.org/10.1097/BOR.0b013e32833bd81f
7. Burger H, van Daele PL, Odding E, Valkenburg HA, Hofman A, Grobbee DE, et al. Association of radiographically evident osteoarthritis with higher bone mineral density and increased bone loss with age. The Rotterdam Study. Arthritis Rheum 1996;39:81-6.
8. Cicuttini FM, Baker J, Hart DJ, Spector TD. Association of pain with radiological changes in different compartments and views of the knee joint. Osteoarthritis Cartilage 1996;4:143-7.
9. Coleman DA, Blair WF, Shurr D. Resection of the radial head for fracture of the radial head. Long-term follow-up of seventeen cases. J Bone Joint Surg Am 1987;69:385-92.
10. Cox LG, van Rietbergen B, van Donkelaar CC, Ito K. Bone structural changes in osteoarthritis as a result of mechanoregulated bone adaptation: a modeling approach. Osteoarthritis Cartilage 2011;19:676-82. https://doi.org/10.1016/j.joca.2011.02.007
11. Dalal S, Bull M, Stanley D. Radiographic changes at the elbow in primary osteoarthritis: a comparison with normal aging of the elbow joint. J Shoulder Elbow Surg 2007;16:358-61. https://doi.org/10.1016/j.jse.2006.08.005
12. Desai SJ, Deluce S, Johnson JA, Ferreira LM, Leclerc AE, Athwal GS, et al. An anthropometric study of the distal humerus. J Shoulder Elbow Surg 2014;23:463-9. https://doi.org/10.1016/j.jse.2013.11.026
13. Ding M, Odgaard A, Hvid I. Changes in the three-dimensional microstructure of human tibial cancellous bone in early osteoarthritis. J Bone Joint Surg Br 2003;85:906-12.
14. Eckstein F, Muller-Gerbl M, Steinlechner M, Kierse R, Putz R. Subchondral bone density in the human elbow assessed by computed

tomography osteoabsorptiometry: a reflection of the loading history of the joint surfaces. J Orthop Res 1995;13:268-78.
15. Edwards WB, Troy KL. Finite element prediction of surface strain and fracture strength at the distal radius. Med Eng Phys 2012;34:290-8. https://doi.org/10.1016/j.medengphy.2011.07.016
16. Felson DT, Cooke TD, Niu J, Goggins J, Choi J, Yu J, et al. Can anatomic alignment measured from a knee radiograph substitute for mechanical alignment from full limb films? Osteoarthritis Cartilage 2009;17:1448-52. https://doi.org/10.1016/j.joca.2009.05.012
17. Goldberg I, Peylan J, Yosipovitch Z. Late results of excision of the radial head for an isolated closed fracture. J Bone Joint Surg Am 1986;68:675-9.
18. Halls AA, Travill A. Transmission of pressures across the elbow joint. Anat Rec 1964;150:243-7.
19. Harris PA, Taylor R, Thielke R, Payne J, Gonzalez N, Conde JG. Research electronic data capture (REDCap)—a metadata-driven methodology and workflow process for providing translational research informatics support. J Biomed Inform 2009;42:377-81. https://doi.org/10.1016/j.jbi.2008.08.010
20. Haverstock JP, Katchky RN, Lalone EA, Faber KJ, King GJ, Athwal GS. Regional variations in radial head bone volume and density: implications for fracture patterns and fixation. J Shoulder Elbow Surg 2012;21:1669-73. https://doi.org/10.1016/j.jse.2012.07.002
21. Hirata Y, Inaba Y, Kobayashi N, Ike H, Yukizawa Y, Fujimaki H, et al. Correlation between mechanical stress by finite element analysis and 18F-fluoride PET uptake in hip osteoarthritis patients. J Orthop Res 2015;33:78-83. https://doi.org/10.1002/jor.22717
22. Hotchkiss RN, Weiland AJ. Valgus stability of the elbow. J Orthop Res 1987;5:372-7.
23. Ike H, Inaba Y, Kobayashi N, Yukizawa Y, Hirata Y, Tomioka M, et al. Effects of rotational acetabular osteotomy on the mechanical stress within the hip joint in patients with developmental dysplasia of the hip: a subject-specific finite element analysis. Bone Joint J 2015;97-b:492-7. https://doi.org/10.1302/0301-620x.97b4.33736
24. Ikeda M, Sugiyama K, Kang C, Takagaki T, Oka Y. Comminuted fractures of the radial head. Comparison of resection and internal fixation. J Bone Joint Surg Am 2005;87:76-84. https://doi.org/10.2106/jbjs.c.01323
25. Kapoutsis CA, Vavoulidis CP, Pitas I. Morphological iterative closest point algorithm. IEEE Trans Image Process 1999;8:1644-6.
26. Kawanishi Y, Miyake J, Kataoka T, Omori S, Sugamoto K, Yoshikawa H, et al. Does cubitus varus cause morphologic and alignment changes in the elbow joint? J Shoulder Elbow Surg 2013;22:915-23. https://doi.org/10.1016/j.jse.2013.01.024
27. Keyak JH, Rossi SA, Jones KA, Skinner HB. Prediction of femoral fracture load using automated finite element modeling. J Biomech 1998;31:125-33.
28. Lindenhovius AL, Felsch Q, Doornberg JN, Ring D, Kloen P. Open reduction and internal fixation compared with excision for unstable displaced fractures of the radial head. J Hand Surg Am 2007;32:630-6. https://doi.org/10.1016/j.jhsa.2007.02.016
29. Mason ML. Some observations on fractures of the head of the radius with a review of one hundred cases. Br J Surg 1954;42:123-32.
30. Matsuura Y, Kuniyoshi K, Suzuki T, Ogawa Y, Sukegawa K, Rokkaku T, et al. Accuracy of specimen-specific nonlinear finite element analysis for evaluation of distal radius strength in cadaver material. J Orthop Sci 2014;19:1012-8. https://doi.org/10.1007/s00776-014-0616-1
31. Miyake J, Shimada K, Moritomo H, Kataoka T, Murase T, Sugamoto K. Kinematic changes in elbow osteoarthritis: in vivo and 3-dimensional analysis using computed tomographic data. J Hand Surg Am 2013;38:957-64. https://doi.org/10.1016/j.jhsa.2013.02.006
32. Miyamura S, Oka K, Abe S, Shigi A, Tanaka H, Sugamoto K, et al. Altered bone density and stress distribution patterns in long-standing cubitus varus deformity and their effect during early osteoarthritis of the elbow. Osteoarthritis Cartilage 2018;26:72-83. https://doi.org/10.1016/j.joca.2017.10.004
33. Morrey BF, An KN. Articular and ligamentous contributions to the stability of the elbow joint. Am J Sports Med 1983;11:315-9.
34. Morrey BF, An KN, Stormont TJ. Force transmission through the radial head. J Bone Joint Surg Am 1988;70:250-6.
35. Morrey BF, Chao EY, Hui FC. Biomechanical study of the elbow following excision of the radial head. J Bone Joint Surg Am 1979;61:63-8.
36. Muller-Gerbl M, Putz R, Hodapp NH, Schulta E, Wimmer B. Computed tomography-osteoaboorptiometry: a method of assessing the mechanical condition of the major joints in a living subject. Clin Biomech (Bristol, Avon) 1990;5:193-8.
37. Oka K, Murase T, Moritomo H, Goto A, Sugamoto K, Yoshikawa H. Accuracy analysis of three-dimensional bone surface models of the forearm constructed from multidetector computed tomography data. Int J Med Robot 2009;5:452-7. https://doi.org/10.1002/rcs.277
38. Ramazanian T, Muller-Lebschi JA, Chuang MY, Vaichinger AM, Fitzsimmons JS, O'Driscoll SW. Effect of radiocapitellar Achilles disc arthroplasty on coronoid and capitellar contact pressures after radial head excision. J Shoulder Elbow Surg 2018;27:1785-91. https://doi.org/10.1016/j.jse.2018.05.022
39. Ring D, Quintero J, Jupiter JB. Open reduction and internal fixation of fractures of the radial head. J Bone Joint Surg Am 2002;84-a:1811-5. https://doi.org/10.2106/00004623-200210000-00011
40. Sharma L, Song J, Felson DT, Cahue S, Shamiyeh E, Dunlop DD. The role of knee alignment in disease progression and functional decline in knee osteoarthritis. JAMA 2001;286:188-95.
41. Shepard MF, Markolf KL, Dunbar AM. Effects of radial head excision and distal radial shortening on load-sharing in cadaver forearms. J Bone Joint Surg Am 2001;83:92-100.
42. van Riet RP, Morrey BF, O'Driscoll SW, Van Glabbeek F. Associated injuries complicating radial head fractures: a demographic study. Clin Orthop Relat Res 2005;441:351-5. https://doi.org/10.1097/01.blo.0000180606.30981.78
43. Wang T, Wen CY, Yan CH, Lu WW, Chiu KY. Spatial and temporal changes of subchondral bone proceed to microscopic articular cartilage degeneration in guinea pigs with spontaneous osteoarthritis. Osteoarthritis Cartilage 2013;21:574-81. https://doi.org/10.1016/j.joca.2013.01.002
44. Willing RT, Lalone EA, Shannon H, Johnson JA, King GJ. Validation of a finite element model of the human elbow for determining cartilage contact mechanics. J Biomech 2013;46:1767-71. https://doi.org/10.1016/j.jbiomech.2013.04.001